Optimisation of two-dimensional undulatory swimming at high Reynolds number

C. Eloy*, L. Schouveiler

IRPHE, CNRS & Aix-Marseille Université, 49 rue Joliot Curie, 13013 Marseille, France

Abstract

The propulsion performance of a flexible plate undergoing an arbitrary harmonic motion in a two-dimensional and inviscid fluid is addressed. This plate being free of external forces, heaving and pitching cannot be imposed and are the results of recoil conditions on the body. Linear unsteady airfoil theory is first used to calculate the average thrust and power required for swimming. The propulsive performance is then discussed in terms of hydrodynamic efficiency, energy consumption and average swimming speed and two different asymptotic regimes are identified: the low-velocity regime and the high-velocity regime. The optimal swimming gaits are calculated in the different regimes as a function of the plate mass ratio and leading-edge suction. Finally an empirical non-linear model is proposed to complement the linear model and the optimal swimming modes are calculated and discussed within this framework. For a fixed number of degrees of freedom, it is found that the Strouhal number of the optimal mode is almost constant, independently of the swimming regime.

Keywords: Undulatory swimming, Potential flow, Fish locomotion

1. Introduction

Aquatic animals have developed different highly efficient propulsion systems. Customarily, a propulsive force is generated by a curvature wave propagating backwards along the swimmer's body. Depending on the envelope of this bending wave, different swimming modes can be distinguished [1–3]. When the amplitude of the undulations is confined to the posterior part of the body the swimming is said to be carangiform and ultimately, the thunniform swimmers, as sharks or tunas, use only the flapping of their caudal fin to be propelled. This swimming mode has been widely studied theoretically [4–8] and experimentally [9–11] as an efficient alternative to the conventional screw propeller . On the contrary, the purely undulatory swimming, referred to as anguilliform, where the amplitude is significant along the whole body has been much less studied except in the limit of very elongated animals [5, 12, 13].

When considering the flapping of a rigid foil, only few parameters control the propulsion, namely the geometric characteristics of the foil (its chord, span and thickness), the flapping frequency, the amplitudes of heaving and pitching and their relative phase difference. Using unsteady airfoil theory [14, 15], the two-dimensional inviscid flow around the foil can be calculated in the limit of small flapping amplitudes. This flow depends on the vorticity formed in the viscous boundary layers attached to the surface of the foil and advected in its wake. Once this flow is known, the pressure difference across the foil can be worked out and this yields the total power required for the motion, the wasted power and the power of the thrust force (which is simply equal to the difference of the two previous powers) [4, 5].

The optimal flapping of a rigid foil has been addressed by Lighthill [5] and Wu [7] independently. They both showed that maximal hydrodynamic efficiency is reached when the phase angle between heave and pitch is close to $\pi/2$. The optimal amplitude ratio (pitching/heaving) and the efficiency are both increasing function of the flapping frequency converging towards one. These predictions have been confirmed by experimental measurements made on oscillating foils towed in a tank [9–11].

Both Lighthill [5] and Wu [7] pointed out that an important contribution to the thrust may originate from the leading-edge suction. This localized force, which is due to the singularity of the pressure field at the leading-edge, may be difficult to realize in practice because it promotes dynamic stall. When stall occurs, vorticity is detached at the leading edge, and a leading-edge vortex is formed. This phenomenon can be dramatic in terms of performance as it has been recognized in experiments [11].

In the present paper, we will address the more general problem of a thin flexible plate undergoing an arbitrary harmonic motion in two dimensions. Heaving and pitching amplitudes will not be prescribed and will arise from the recoil conditions on the body (Newton's second law). This anguilliform swimming mode is relevant to elongated animals like eels (for which an elongated-body theory [5] is also appropriate), rays or in the prospect of developing highly efficient bio-inspired propulsion systems [16, 17].

The structure of the paper is the following. We will first reproduce the main results of unsteady airfoil theory applied to the present swimming problem by following Wu [7] to deduce the dimensionless thrust, power required and power wasted

*Corresponding author
Email address: eloy@irphe.univ-mrs.fr (C. Eloy)

as a function of the parameters of the problem. The optimal swimming motions will then be calculated and discussed in the framework of this linear model. We will then introduce an empirical non-linear model and show how the optimal swimming gaits are modified. Finally, we will discuss these results in the context of fish swimming.

2. Formulation of the problem

2.1. Plate deformation

Consider the harmonic deformation with angular frequency Ω of a flexible plate of length $2L$ and zero thickness in a two-dimensional inviscid and incompressible fluid (Fig. 1). The transverse deformation of the plate produces a longitudinal instantaneous thrust force T. In the cruising regime, when this force is averaged over one period, it is equilibrated by the average drag D and yield an average swimming velocity U .

Choosing the frame of reference moving with the plate at velocity U and using the half-chord L and the angular frequency Ω as characteristic length and frequency to formulate the problem in dimensionless form (with lowercase letters), the plate deformation may be prescribed by

$$y(x,t) = h(x)\,\mathrm{e}^{\mathrm{i}t} \quad (-1 < x < 1), \tag{1}$$

where $h(x)$ is a continuous function assumed to be small at this point, i.e. $h \ll 1$ and $\partial h/\partial x \ll 1$. In this dimensionless form, the flow velocity is now $u = U/(\Omega L)$. Note that the reduced frequency k, commonly used in aerodynamics, is the inverse of the dimensionless velocity: $k = 1/u = \Omega L/U$.

The plate motion is expanded onto the eingenmodes of an elastic beam in vacuo with free-free boundary conditions

$$h(x) = \sum_{n=1}^{N} a_n h_n(x), \tag{2}$$

with $h_1(x) = 1$, $h_2(x) = x$, and $h_n(x)$, the n-th eigenmode given explicitly in the Appendix. This expansion ensures that no internal force or torque have to be applied at the free ends of the plate. The first two eigenmodes $h_1(x)$ and $h_2(x)$ correspond to heave and pitch motions and play a particular role as it will be shown below. Note also that these eigenmodes form a complete orthogonal set of the functions with free-free boundary conditions. In the following, the number N of eigenmodes used in the expansion will be an adjustable parameter. This expansion is therefore compatible with an actuated elastic plate with a small number of degrees of freedom. However, the way the plate would have to be actuated will not be discussed in this paper and its motion will be prescribed.

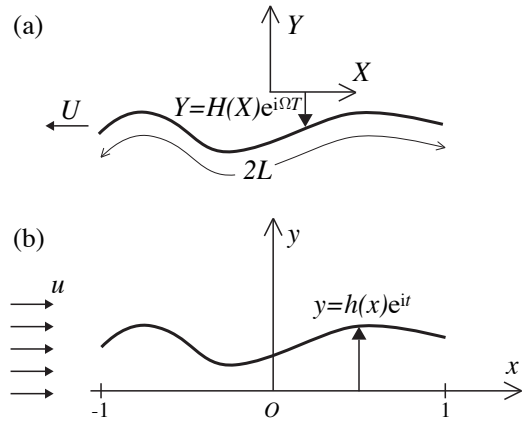

Figure 1: Sketch of the swimming flexible plate: (*a*) in dimensional units and (*b*) in dimensionless units and in the frame of reference moving at velocity U.

Following Wu [4, 6, 7] with slightly different notations, the swimming performances are evaluated by expanding the plate motion as

$$h(x) = \frac{b_1}{2} + \sum_{n=1}^{\infty} b_{n+1}\cos n\theta \quad (x = \cos\theta), \tag{3}$$

where $0 < \theta < \pi$ (see Eq. (2) in Wu [7]). It correspond to a decomposition of $h(x)$ onto the Chebyshev polynomials of the first kind. For small deformations, the transverse flow velocity on the plate is

$$v(x) = \frac{\partial y}{\partial t} + u\frac{\partial y}{\partial x} = u\left(\mathrm{i}kh + \frac{\partial h}{\partial x}\right)\mathrm{e}^{\mathrm{i}t}, \tag{4}$$

which is also expanded onto the Chebyshev polynomials of the first kind such that

$$\mathrm{i}kh + \frac{\partial h}{\partial x} = \frac{c_1}{2} + \sum_{n=1}^{\infty} c_{n+1}\cos n\theta, \tag{5}$$

(see Eq. (4) in Wu [7])

The link between the expansion onto the beam eigenmodes given by Eq. (2) and the expansion onto the Chebyshev polynomials of Eqs. (3) and (5) can be expressed vectorially

$$\mathbf{b} = \mathbf{B}\cdot\mathbf{a}, \quad \mathbf{c} = \mathbf{C}\cdot\mathbf{a} \tag{6}$$

where the matrix coefficients of $\mathbf{B}$ and $\mathbf{C}$ are given by

$$B_{ij} = \frac{2}{\pi}\int_0^{\pi} h_j(x)\cos(i-1)\theta\,\mathrm{d}\theta, \tag{7}$$

$$C_{ij} = \frac{2}{\pi}\int_0^{\pi}\left(\mathrm{i}kh_j + \frac{\partial h_j}{\partial x}\right)\cos(i-1)\theta\,\mathrm{d}\theta, \tag{8}$$

and $\mathbf{a}$, $\mathbf{b}$ and $\mathbf{c}$ are the column vectors containing the different a_n, b_n and c_n respectively. As it will appear below (see also the discussion in Wu [7]), only the first four components of $\mathbf{b}$ and $\mathbf{c}$ are needed to evaluate the swimming performance. Hence, $\mathbf{B}$ and $\mathbf{C}$ will be $4 \times N$ matrices in the following.

2.2. Perturbation flow

When the flow around the plate is assumed to be potential, the perturbation flow is found by solving the Laplace equation for the perturbation velocity potential with a prescribed transverse velocity given by Eq. (4) on the plate (which is a Neumann boundary for the velocity potential). This calculation is classical in unsteady aerodynamics [14, 15, 18, 19] and has also been used in the context of flapping foils [4–7].

When the problem is linearized, the distribution of vorticity in the plate depends linearly of the transverse flow velocity imposed on the plate. The flow being potential, the vorticity can only be generated in the viscous boundary layers attached to the plate surface. This vorticity is then shed in the wake at the trailing edge. In the linear limit, the vorticity is advected in the x-direction at the velocity u. The problem being time-periodic with a period 2π in dimensionless form, it results a space-periodic wake formed of vortex sheet along the Ox-axis with a wavelength $\lambda = 2\pi u$.

It is interesting to note that in swimming experiments, the wake behind the swimmer is a von Kármán wake when drag dominates and a reverse von Kármán wake when thrust dominates [20]. At the transition between these two regimes, the wake is formed of aligned vortices of alternate signs, very similar to the wake of the present linear potential theory.

For the sake of brevity and clarity, the calculation of the perturbation flow and perturbation pressure will not be detailed here and the readers interested in these details are referred to the above references.

2.3. Recoil conditions

If the flexible plate propels itself without external agencies, Newton's second law apply. This recoil condition require that the hydrodynamic lift and moment must be equal to the rate of change of the lateral and angular momentum of the body [6, 7]. Expressed vectorially, it follows that

$$\mathbf{l}(k)\cdot\mathbf{c} = \frac{k^2}{\pi}\,\mathbf{L}\cdot\mathbf{a}, \tag{9}$$

$$\mathbf{m}(k)\cdot\mathbf{c} = -\frac{2k^2}{\pi}\,\mathbf{M}\cdot\mathbf{a}, \tag{10}$$

where the row vectors $\mathbf{l}$ and $\mathbf{m}$ only depend on the reduced frequency k and are given in the Appendix (see Eqs. (15–16) in Wu [7]).

The row vectors $\mathbf{L}$ and $\mathbf{M}$ are given by

$$L_i = \int_{-1}^{1} m(x)h_i(x)\,\mathrm{d}x, \tag{11}$$

$$M_i = \int_{-1}^{1} xm(x)h_i(x)\,\mathrm{d}x, \tag{12}$$

where $m(x)$ is the dimensionless mass per unit length of the plate (using ρL as the reference mass per unit length, with ρ the fluid density). We will assume that $m(x)$ is semi-elliptic in this paper

$$m(x) = \mu\sqrt{1-x^2}, \tag{13}$$

and μ will be called the mass ratio. For a swimmer with same density as water, the maximum thickness-to-length ratio is $\mu/2$. In the following the value $\mu = 0.3$ will be used, corresponding to an aspect ratio of 6.7, close to the values measured in most fish and cetacean species. The specific distribution of mass (semi-elliptic here) is not an important aspect of the problem: other distributions have been tested without affecting the results qualitatively.

The Eqs. (9) and (10) expressing Newton's second law allows to calculate the amplitudes a_1 and a_2 corresponding to heaving and pitching respectively as a functions of the other amplitudes a_n. In other words, when the swimmer prescribes a certain bending along its length, its transverse motion (heave) and rotation (pitch) are the result of the recoil conditions. It can thus be concluded that the number of degrees of freedom is $N-2$, where N is the number of eigenmodes in Eq. (2).

2.4. Propulsion performance

The time averages of thrust $\langle T\rangle$, energy loss $\langle E\rangle$ and power required $\langle P\rangle$ can be put in dimensionless form following Wu again [4, 6, 7]

$$C_E = \langle E\rangle/\left(\tfrac{1}{4}\pi\rho U^3 L\right) = \mathbf{a}^*\cdot\mathbf{E}(k)\cdot\mathbf{a}, \tag{14}$$

$$C_P = \langle P\rangle/\left(\tfrac{1}{4}\pi\rho U^3 L\right) = \mathbf{a}^*\cdot\mathbf{P}(k)\cdot\mathbf{a}, \tag{15}$$

$$C_T = \langle T\rangle/\left(\tfrac{1}{4}\pi\rho U^2 L\right) = C_P - C_E, \tag{16}$$

where $\mathbf{a}^*$ denotes the adjoint of $\mathbf{a}$ (see Eqs. (6–8) in Wu [7]). Under this form, it is evident that the above coefficients are quadratic forms of the amplitude vector $\mathbf{a}$.

When the plate is swimming at constant average speed, the average thrust $\langle T\rangle$ has to be opposite to the average drag $\langle D\rangle$. If the flow is potential or if the viscous stresses are negligible (which is generally the case), the drag is also proportional to ρU^2 and therefore in dimensionless form this conditions reduces to

$$C_T = C_D = \langle D\rangle/\left(\tfrac{1}{4}\pi\rho U^2 L\right), \tag{17}$$

where the drag coefficient C_D only depend on the swimmer shape. In the following, the drag coefficient will be assumed to be constant, $C_D = 10^{-2}$. This value is relatively high for a streamlined body, but the results do not qualitatively depend on the particular value chosen.

If the thrust has to counterbalance the drag on average, the instantaneous values do not generally balance. This leads to small accelerations and decelerations over each period. However, when body inertia is present, these accelerations can be neglected and the instantaneous velocity is always equal to the average velocity at leading order.

The propulsion performance is usually measured with the hydrodynamic efficiency η, defined as the ratio of the power generated by the thrust to the total power required

$$\eta = \frac{C_T}{C_P} = \frac{C_D}{C_P} = 1 - \frac{C_E}{C_P}. \tag{18}$$

An alternative approach is to examine two quantities: the average swimming velocity and the consumption of energy per unit distance. In dimensionless form, these quantities reduce to the dimensionless velocity $u = 1/k$ and the dimensionless consumption ξ given by

$$\xi = \langle P/U\rangle/\left(\tfrac{1}{4}\pi\rho\Omega^2 L^3\right) = \frac{C_P}{k^2} = \frac{C_D}{\eta k^2}, \tag{19}$$

where P/U is the instantaneous hydrodynamic energy consumption per unit distance at leading order.

When the angular frequency Ω is constant, the swimmer reaches a large velocity when the reduced frequency k is small.

But in this case, the consumption is large as ξ scales as k^{-2} (assuming that C_D is constant and η of order one). Therefore, two asymptotic regimes can be distinguished: a *high-velocity regime* for asymptotically small k which implies a large consumption, and a *low-velocity regime* for large k which implies a low consumption. Moderate values of k will correspond to the *intermediate regime* and the value $k = \pi$ will be chosen to describe this regime as it corresponds to a swimming velocity of one body length per period.

2.5. Leading-edge suction

The leading-edge suction S is the local thrust force arising from the singularity of the pressure at the leading edge. This force is never negligible and can be greater than the total thrust in some cases (the complementary thrust coming from the rest of the plate thus being negative). In dimensionless form, the average leading-edge suction can be calculated similarly to the total thrust

$$C_S = \langle S \rangle / \left(\tfrac{1}{4}\pi\rho U^2 L\right) = \mathbf{a}^* \cdot \mathbf{S}(k) \cdot \mathbf{a}, \tag{20}$$

where the matrix $\mathbf{S}$ is given in the Appendix.

It has been recognized that a large leading-edge suction may be hard to achieve in practice [5, 7, 11]. In such cases, one expects dynamic stall to occur, an ubiquitous phenomenon in helicopter flight and turbomachines which can limit or enhance the performances. In this case, a leading-edge vortex is detached and the hydrodynamic forces can no longer be described with the present potential flow theory. Some animals have also been shown to exploit the flow separation at the leading edge, in particular in flapping flight [21]. However, the phenomenon of dynamic stall is difficult to model adequately and the existing model usually consider rigid plates in steady flow [22].

It is beyond the scope of the present paper to develop a model of dynamic stall for a flexible plate in unsteady flow. Instead, the leading-edge suction will be constrained to zero which is possible for a large enough number of degrees of freedom ($N - 2$). When $C_S = 0$, the flow is almost parallel to the plate at the leading-edge in such a way that the pressure field is no longer singular at this point. One could alternatively impose the flow to be parallel to the plate at the leading edge by using the decomposition given by Eq. (3), which would results in C_S being close to zero. Finally, another way to prevent large leading-edge suction would be to add the constrain $C_S < C_T$ such that the thrust originating from the rest of the plate remains positive. These three alternatives have been tested and they give very similar results.

3. Optimization of the linear problem

In this section, optimal plate deformations will be calculated for the different swimming regimes. This optimization procedure consists in finding the minimum of the dimensionless energy loss C_E given by Eq. (14) as a function of the reduced frequency k when the the amplitude vector $\mathbf{a}$ is varied.

This optimization is constrained by the recoil conditions of Eqs. (9) and (10) and by the balance of thrust and drag given by Eq. (17). Since the thrust and energy averages are quadratic functions of the amplitude vector $\mathbf{a}$, its norm C_N will be also constrained, where

$$C_N = \sum_{n=3}^{N} |a_n|^2 . \tag{21}$$

Note that the heave ($n = 1$) and pitch ($n = 2$) amplitudes are omitted in this norm since they are assumed to depend passively on the other amplitudes via the recoil conditions as explained above.

This optimization depends on the free parameters of the problem: the normalized drag C_D/C_N, the mass ratio μ given by Eq. (13), the number of modes N, the reduced frequency k and the values allowed for the leading-edge suction C_S. In this section, the values of the drag and norm will be fixed: $C_D = C_N = 10^{-2}$ and the number of modes will be set to its minimum to allow for the constraints: $N = 5$. The main reason for keeping the value of N small is that, for larger values, the optimal deformation can locally exhibit large angles with the main flow and therefore escape the validity domain of the linear model. The dependence on the number of modes will be discussed with an appropriate non-linear model in the next section.

The function to minimize and the different constraints can all be expanded as polynomials of the amplitudes a_n. This property allows to find the global optimum for a given reduced frequency k with a symbolic calculation software such as Mathematica [23].

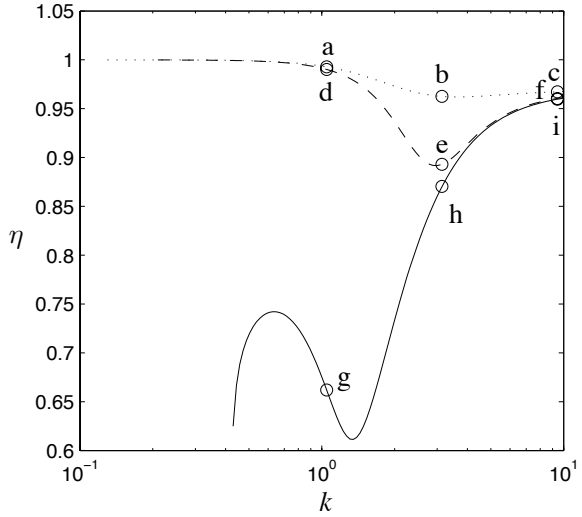

Figure 2: Efficiency as a function of the reduced frequency for the linear model. The parameters are $C_D = C_N = 10^{-2}$, $N = 5$ and: $C_S \neq 0$, $\mu = 0$ (dotted line); $C_S = 0$, $\mu = 0$ (dashed line), $C_S = 0$, $\mu = 0.3$ (solid line). The circles refer to the optimal gaits illustrated in Fig. 3.

3.1. Leading-edge suction

For a massless flexible plate (i.e. $\mu = 0$, equivalent to a negligible thickness) and with a unconstrained leading-edge suction, the optimal efficiency has been calculated as a function of the

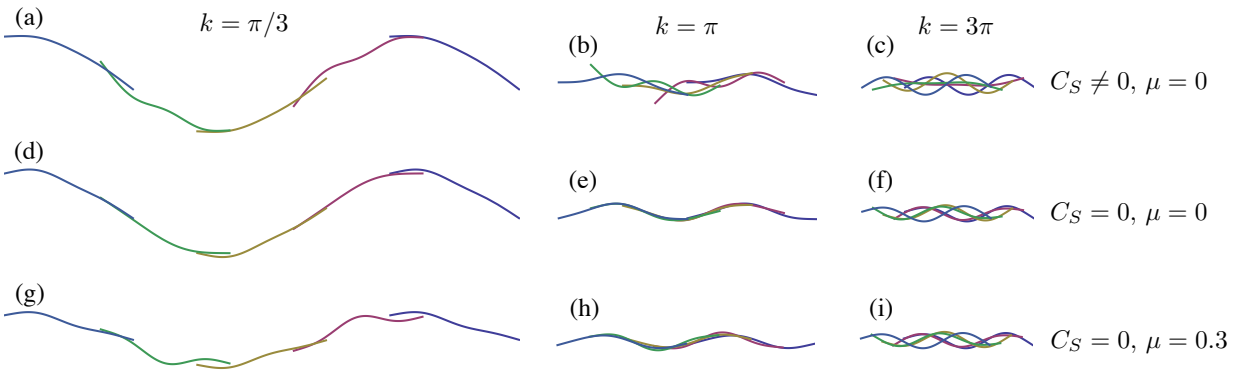

Figure 3: Optimal swimming gaits given by the linear model for $C_D = C_N = 10^{-2}$, $N = 5$ and different reduced frequencies k as labelled. The plate is moving from right to left and three instantaneous deformations are pictured per period (with no vertical magnification). The hydrodynamic efficiency associated with each of these gaits is given in Fig. 2.

reduced frequency (Fig. 2, dotted line). The corresponding optimal swimming gaits for $k = \pi/3$, π and 3π are reproduced in Fig. 3 (a–c). In the following, we will refer to these particular values of the reduced frequency as the high-velocity, intermediate and low-velocity regimes respectively.

In these three regimes, the leading-edge suction far exceeds the total thrust: $C_S = 4.9C_T$, $18.5C_T$ and $23C_T$ respectively. It means that the contribution of the thrust originating from the rest of the plate is negative. Since such a large leading-edge suction would be difficult to realize without dynamic stall, we have calculated the optimal swimming gaits with the additional constraint of zero leading-edge suction, with C_S given by Eq. (20).

The resulting efficiency is plotted in Fig. 2 with a dashed line. As expected intuitively, the efficiency is lower with this additional constraint. This is especially true in the intermediate regime when $k \approx \pi$. The corresponding optimal swimming gaits (see Figs. 3 b,e) indeed show different features in this regime. When the leading-edge suction is zero the plate follows an undulating path such that the leading edge is always parallel to its local velocity (this is also true for any point of the plate). When C_S is non zero, the leading edge is no longer parallel to its velocity (Fig. 3 b) and the optimal gait looks 'anomalous'.

In the high-velocity regime ($k \lesssim 1$), whether the leading-edge suction is constrained to zero or not, the optimal swimming gaits exhibits the same characteristics and the efficiency is almost equal to 100%. The amplitudes of heave and pitch dominate over the bending amplitudes and the path followed by the leading edge is a large amplitude sine curve (with this amplitude increasing as k decreases). Note that there is no solution for $k < 0.22$ when the leading-edge suction is constrained to zero (and for $k < 0.13$ without this constraint). This means that there is a maximum allowed speed in this case $u = 1/k = 4.5$. This maximum speed is the consequence of the imposed norm $C_N = 10^{-2}$ as defined by Eq. (21). Note that the maximum velocity would be drastically reduced if the heave and pitch amplitudes were included in the definition of the norm C_N.

In the low-velocity regime ($k \gtrsim 10$) , the optimal gaits are very similar whether the leading-edge suction is constrained to zero or not (Fig. 3 c,f). In this regime, the heave and pitch amplitude are almost zero and the deformation is approximately given by a sine function such that there are 1.5 wavelengths along the chord (there is 1 wavelength when $k = \pi$ and approximately $1/3$ wavelength with $k = \pi/3$). This particular deformation and wavelength is constrained by the relatively small number of degrees of freedom allowed ($N = 5$).

Since an unconstrained leading-edge suction leads to large values of C_S and mostly to negative values of the thrust originating from the rest of the plate surface, we will always add the additional constraint of zero leading-edge suction in the following.

3.2. *Effects of body inertia*

We now examine the effect of body inertia on the swimming performance by considering a mass ratio $\mu = 0.3$, still with zero leading-edge suction (i.e. $C_S = 0$). The mass per unit chord as given by Eq. (13) reflects a swimmer of elliptical thickness with the same density as the surrounding fluid and with an aspect ratio AR $= \mu/2 = 0.15$ (defined as the maximum thickness at mid chord divided by the chord).

The hydrodynamic efficiency of this elliptical swimmer is plotted as a function of the reduced frequency in Fig. 2 with a solid line, and the corresponding optimal gaits are illustrated in Fig. 3 (g–i). The main difference with the massless swimmer is that it is less efficient in the high-velocity regime with a hydrodynamic efficiency dropping to $\eta \approx 0.65$ and a maximum speed of $u = 1/k = 2.4$ (again this maximum speed is closely related to the imposed norm $C_N = 10^{-2}$). The main reason for the loss of efficiency is that the effects of body inertia prevents large heave and pitch amplitudes and therefore the large-amplitude undulating path followed by the massless swimmer (Fig. 3 d) can no longer be achieved with inertia.

In the intermediate and low-velocity regimes, the optimal gaits and the efficiency are similar with that of the massless swimmer because heave and pitch are small in these regimes.

3.3. *Energy consumption*

The dimensionless energy consumption as defined by Eq. (19) is plotted as a function of the reduced frequency in Fig. 4.

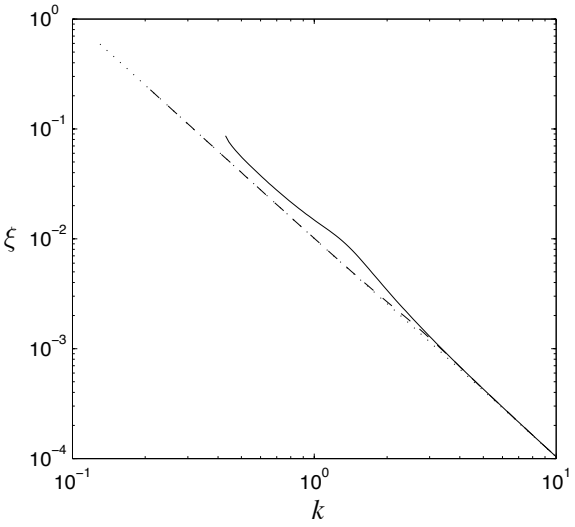

Figure 4: Energy consumption as a function of the reduced frequency for the same parameters as in Fig. 2.

In all cases (with zero or non-zero leading-edge suction, with inertia or not), the consumption is a monotonically decreasing function of the reduced frequency, and therefore a monotonically increasing function of the cruising velocity.

If the swimming performance is evaluated in terms of both consumption and swimming speed, Fig. 4 thus shows that there is no particular value of the reduced frequency for which there is an advantage on both of these criteria compared to the other values. It means the choice of the reduced frequency is always a trade-off between consumption and speed.

It should be pointed out here that the above argument on the reduced frequency and the different swimming regimes assumes that the swimmer deforms itself with a fixed angular frequency Ω. If one allows this frequency to be varied, the swimmer can adjust it in order to obtain any particular value of the reduced frequency for a given targeted swimming velocity. In this case, there will always be an energetic advantage to maximize the hydrodynamic efficiency.

4. Non-linear effects

The major drawbacks of the linear model described above are the following. First, the amplitude of the plate deformation has to be prescribed to perform the optimization as the thrust and energy loss grows are quadratic forms of the plate amplitude. As it has been seen above, this arbitrarily imposed norm C_N yields a maximum swimming velocity. Second, when calculating the optimal swimming gaits with a large number of degrees of freedom, the linear model predicts unrealistic deformations where small wavelength modes have large amplitudes and lead to large angles between the plate and the flow locally. To avoid these drawbacks and to take into account the saturation of both the thrust and the energy loss as the amplitude of the plate deformation grows, we propose here an empirical non-linear model.

4.1. Model

The sources of non-linearities are manifold in this problem. For instance, the thrust is obtained by integrating $p(x)\sin\theta(x)$ along the plate chord, where p is the pressure difference across the flexible plate and θ is the angle between the plate and the horizontal. One source of non-linearity here is the difference between $\sin\theta$ and the x-derivative of the deformation used in the linear approximation which gives at second order (with real quantities now)

$$\sin\theta = \frac{\mathrm{d}h}{\mathrm{d}x}\left(1 - \frac{1}{2}\left(\frac{\mathrm{d}h}{\mathrm{d}x}\right)^2 + \cdots\right). \tag{22}$$

For high-order bending modes, the derivative $\mathrm{d}h/\mathrm{d}x$ scale as $n|a_n|$ in first approximation, where n is the order of the mode.

The other source of non-linearity arises from the saturation of the pressure difference p for large deformations. To find this pressure difference, the velocity potential is first found by solving a Laplace equation with the Neumann boundary condition given by the kinematic boundary condition on the plate surface. This boundary condition states that the normal flow velocity should equal the normal plate velocity. When the deformation amplitude is finite, this Neumann boundary condition has to be applied away from the Ox axis and yield again to a geometric non-linearity for the pressure difference of the form

$$p(x) = p_L\left(1 - \alpha\left(\frac{\mathrm{d}h}{\mathrm{d}x}\right)^2 + \cdots\right), \tag{23}$$

where p_L is the pressure difference of the linear model and α a coefficient which depends a priori on the particular mode of deformation and on the reduced frequency. Note that the sign of the coefficient α is not necessarily positive.

Finally, as it has been shown by Chopra [24], the finite amplitude of the vortex sheet deformation in the wake leads to a non-linearity of the pressure difference of the form

$$p(x) = p_L\left(1 - \beta k^2|a|^2 + \cdots\right), \tag{24}$$

where β is a positive parameter. This particular non-linear term is due to the fact that the wake has a finite thickness that scales as $|a|$ and a wavelength as $\lambda = 2\pi/k$.

To avoid too many empirical coefficients, we propose the following non-linear model, where the dimensionless energy loss, power required and average thrust are now given by

$$C_E = \left(1 - \alpha_E k^2 C_{NL}\right)\mathbf{a}^* \cdot \mathbf{E} \cdot \mathbf{a}, \tag{25}$$

$$C_P = \left(1 - \alpha_P k^2 C_{NL}\right)\mathbf{a}^* \cdot \mathbf{P} \cdot \mathbf{a}, \tag{26}$$

$$C_T = C_P - C_E, \tag{27}$$

where C_{NL} is the following norm

$$C_{NL} = \sum_{n=1}^{N} n^2 |a_n|^2, \tag{28}$$

$\alpha_E = 0.04$ and $\alpha_P = 0.08$ are two empirical coefficients, and the recoil conditions given by Eqs. (9) and (10) are supposed to be unchanged.

When the deformation amplitude is small enough such that $C_{NL} \ll 1$, the linear model is recovered. When the amplitude increases the proposed non-linear model predicts the saturation of the thrust with a non-linear term that grows quadratically both with the reduced frequency (as predicted by the non-linearity due to the wake finite thickness) and with the order of the mode n (as predicted by geometric non-linearities). For asymptotically small reduced frequencies however, the proposed model probably underestimate the non-linearities as the added non-linear term vanishes for vanishing reduced frequency. Each eigenmode contributes to the saturation independently in this model and no interactions between modes are considered.

The present non-linear model is very crude but has several advantages. First, it is very simple and allows to perform a global optimization since the thrust and power coefficients are still given as polynomials of the amplitudes a_n. Second, it captures some essential features of the non-linear saturation such as the dependence on the reduced frequency and on the mode order (which is essential to prevent high-order modes to dominate). Finally, this model has only two adjustable parameters α_E and α_P. The results do not depend appreciably on the value of the coefficient α_E as long as it is significantly lower than α_P. For instance, this parameter could be taken to be zero without notable differences in the following calculations.

The value chosen for the coefficients α_E and α_P are an order of magnitude larger than what can be estimated from the analytical results of Chopra [24] for a heaving and pitching rigid plate, which gives $\alpha_P \approx 0.003$. They are also larger than what can be estimated from the theoretical/numerical results of Anderson *et al.* [25] also on a oscillating rigid plate: $\alpha_P \approx 0.02$. One of the reason to choose larger values in the present study is that the amplitude of the swimming modes and their Strouhal number is closer to what is observed in nature with these values. It could be also argued that for a plate of finite span, an additional energy is loss by the drag affecting the plate lateral displacement. This drag can be estimated to be proportional to the square of the lateral velocity and thus scales as $|a_n|^2$. If one were to choose smaller values for α_E and α_P, it would only increase the amplitude of the optimal swimming mode without qualitatively modifying its dependence on the reduced frequency and on the number of degrees of freedom.

4.2. Results

Using this non-linear model, we have performed optimization calculations keeping the drag coefficient constant ($C_D = 10^{-2}$), the mass ratio constant ($\mu = 0.3$) and increasing the number N of modes of the decomposition starting with the minimal value $N = 5$. The resulting optimal efficiencies are plotted as a function of the reduced frequency in Fig. 5 and the corresponding optimal swimming gaits are illustrated in Fig. 6.

The intuitive feature that the hydrodynamic efficiency should increase as the number of degrees of freedom increases is recovered by the model. Another feature, less intuitive, is that the efficiency globally increases when the reduced frequency decreases (or the swimming velocity increases) reaching values close to 100% when $k \lesssim 1$. This is very different from the linear model where it was the opposite (Fig. 2, solid line). The other difference is that there is no minimum reduced frequency, and thus no maximal dimensionless velocity allowed, the only limit being the prohibitive energetic cost for asymptotically large velocities. This point would probably be different with a non-linear model adapted to asymptotically small values of k.

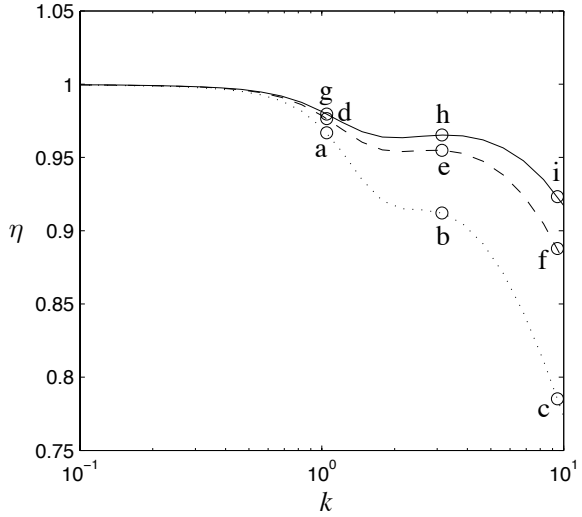

Figure 5: Efficiency as a function of the reduced frequency for the non-linear model. The parameters are: $C_D = 10^{-2}$, $\mu = 0.3$, $N = 5$ (dotted line), $N = 7$ (dashed line), $N = 9$ (solid line), and the circles refer to the optimal gaits plotted in Fig. 6.

The optimal gaits in the different swimming regimes for $N = 5$ (Fig. 6 a–c) share some properties with what was observed in the linear model for the same number of modes (Fig 3 g–i). The amplitude of heaving and pitching also decreases as the reduced frequency increases, but in the non-linear model, the amplitude of all modes decrease as the non-linearity grows as k^2 and thus the amplitude, as defined by the norm C_N given by Eq. (21), is expected to decrease as k^{-2}. For the intermediate regime and with a small number of degrees of freedom (Fig. 6 b), the swimmer follows approximately a undulating path similarly to what was obtained in the linear model (Fig 3 b). However, in the high-velocity regime (Fig. 6 a), the optimal gait is somehow different and consists in a 'kink' propagated backwards by the swimmer. In the low-velocity regime (Fig. 6 c), the optimal gait is again an undulation with approximately 1.5 wavelengths along the plate chord similarly to the linear case (Fig. 3 c) but with a smaller amplitude.

In the non-linear model maximum efficiency is achieved when the reduced frequency is small while the opposite is true in the linear model when body inertia is taken into account. This difference arises from the fact that the norm C_N is fixed in the linear model whereas it is free and varies roughly as k^{-2} in the non-linear model.

When the number of modes is increased, swimming is more efficient and this gain in efficiency is reflected in the optimal swimming gaits. For the intermediate regime for instance (Fig. 6 b,e,h), as N is increased, the amplitude of the undulat-

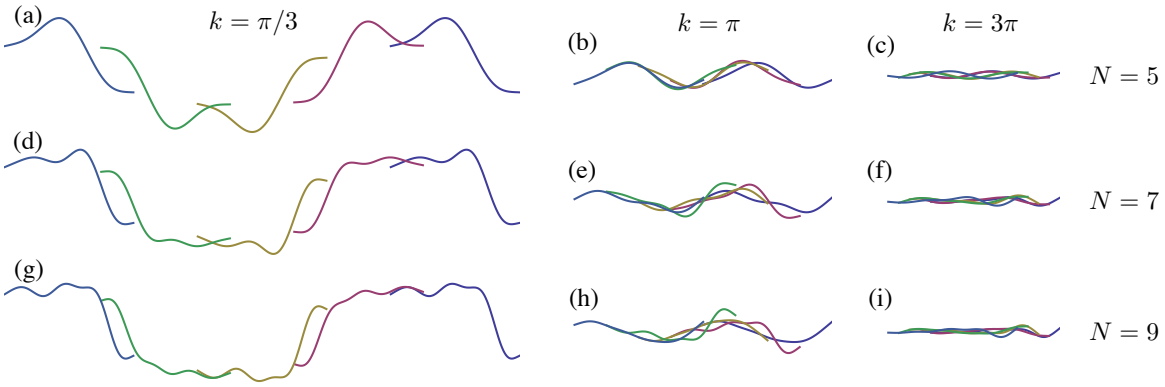

Figure 6: Optimal swimming gaits given by the non-linear model for $C_D = 10^{-2}$, $C_S = 0$, $\mu = 0.3$. The reduced frequency k and the number of modes N are varied as labelled. The hydrodynamic efficiency and the Strouhal number associated with each of these gaits are given in Figs. 5 and 7.

ing path followed by the leading edge is reduced whereas the amplitude at the trailing edge is increased. The optimal mode envelope thus exhibits a maximum at the tail which is more pronounced as N increases. This can be related to the result of Lighthill [5] using elongated-body theory which shows that the confinement of undulations to a reduced fraction of the fish's length near the caudal fin should produce a gain in efficiency. The hypotheses used by Lighthill are very different from the present work because elongated-body theory assumes that the fish span is small compared to its length, and he also assumes that the lateral fish motion generates a drag due to vortex shedding. However, the conclusion is similar and suggests that confining the deformation near the trailing edge leads to more efficient swimming for all aspect ratios.

4.3. Strouhal number

From the above calculations of optimal swimming gaits, we have evaluated the corresponding Strouhal number defined as

$$\mathrm{St} = \frac{\Omega A}{2\pi U} = \frac{k}{\pi}\left|\sum_{n=1}^{N} a_n h_n(1)\right|, \tag{29}$$

where A is the peak-to-peak amplitude at the trailing edge. The results are plotted as a function of the reduced frequency in Fig. 7.

For a given N, and over a wide range of the reduced frequency ($1 \lesssim k \lesssim 10$), the Strouhal number is almost constant: $\mathrm{St} \approx 0.15$ for $N = 5$; $0.2 < \mathrm{St} < 0.25$ for $N = 7$; $0.25 < \mathrm{St} < 0.3$ for $N = 9$. This is probably due to the particular form of the non-linear term chosen in the model which induces that $k^2 C_{NL}$ should be almost constant such that the thrust saturates (indeed the calculations show that $k^2 C_{NL} \approx 4$ over the whole range of k). And therefore the amplitudes a_n should decrease as k^{-1}. However, the fact that the Strouhal number is almost constant does not reflect that the high-velocity regime is dominated by heaving and pitching whereas the low-velocity regime is dominated by the higher order modes.

When the number of modes N increases, the Strouhal number increases also, showing again that high efficiency favors a plate deformation with large deformation near the trailing edge. We

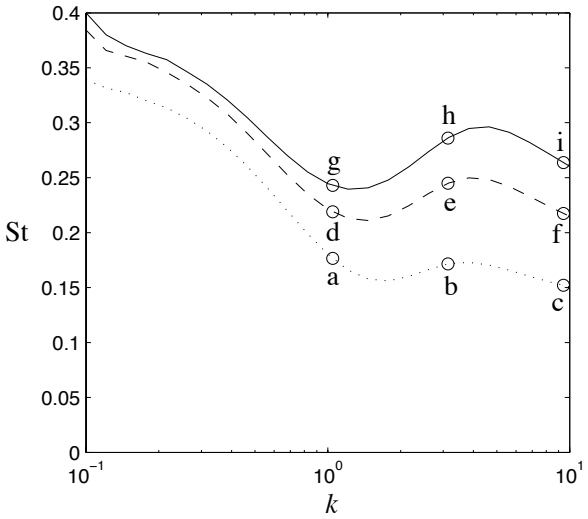

Figure 7: Strouhal number as a function of the reduced frequency. Same parameters as Fig. 5.

have performed calculations in the intermediate regime ($k = \pi$) with N up to 15 (not plotted here) and they show that the Strouhal number grows monotonically up to $\mathrm{St} = 0.35$ without clear signs of saturation.

Surprisingly, the Strouhal numbers obtained with the present simple model for $N \geq 7$ falls within the range of Strouhal numbers measured on swimming [26, 27] and flying [28] animals: $0.2 < \mathrm{St} < 0.4$. Indirectly, this supports the belief that animal locomotion is tuned for high hydrodynamical efficiency.

5. Discussion

In this paper, the propulsion performance and the optimization of a flexible plate undergoing a harmonic motion have been addressed. When this plate is free of external forces, its heave and pitch motions are found by using recoil conditions and thus are the results of its particular bending deformation. Using a linear model based on potential flow theory, the aver-

age thrust power and wasted power can be calculated explicitly and an optimization procedure can be performed. Different optimal swimming regimes have been identified: a low-velocity regime in which the energy consumption is small, a high-velocity regime implying a large energy consumption and an intermediate regime. We have shown that constraining the leading-edge suction to zero, in order to avoid dynamic stall, the optimal swimming gaits consist in an undulation of the plate with the number of wavelength along the plate chord increasing as the reduced frequency increases (corresponding also to a decrease of both the swimming velocity and energy consumption). We have also shown that taking into account the effects of body inertia reduces the hydrodynamic efficiency, particularly in the high-velocity regime (for asymptotically small reduced frequencies).

An empirical non-linear model has also been proposed to model the amplitude saturation in swimming. This simple model allows to find optimal swimming gaits for the different regimes which are close to what is observed in nature. In particular, it is shown that a gain in efficiency is obtained when allowing a larger number of degrees of freedom, the resulting gait having a larger deformation near the trailing edge. The Strouhal number of these swimming modes have also been calculated and is found to lie in the interval $0.2 < \mathrm{St} < 0.4$ for all swimming regimes, as it has been measured on swimming and flying animals [26–28]. With more numerical or experimental data on the propulsion of undulating plates, a more refined model could certainly be developed, giving a better insight into the physical mechanism of swimming but probably at the cost of simplicity.

The present study being two-dimensional, one possible refinement would be to take into account the three-dimensional effects on the swimming efficiency. This has been done by Chopra [29] on oscillating foils of different planforms. The major effect is that the average pressure along the span is lower than what is to be expected from a two-dimensional calculation, in agreement with unsteady airfoil theory [19, 30]. In the case of a flexible plate, a similar effect has been mentioned by the authors in another context [31, 32]. On that account, the thrust should be lower when taking into account the three-dimensional effects but the picture should be qualitatively unchanged.

One possible application of the present theoretical study would be to address the swimming mechanism of animals like rays for which a two-dimensional approach seems appropriate. One particularity of these animals however is that they usually swim very close to the sea floor. It would be interesting to understand how the presence of this near wall modifies the swimming performance and if the optimal swimming gaits are different in this case.

Acknowledgements. This work was sponsored by the French ANR under the project ANR-06-JCJC-0087.

Appendix A.

Appendix A.1. Eigenmodes

The eigenmodes of an elastic beam in vacuo are given by

$$h_n(x) = \cos k_n x + \cosh k_n x + \gamma_n (\sin k_n x + \sinh k_n x) \quad (n \geq 3), \tag{A.1}$$

with

$$\gamma_n = \frac{\cosh k_n - \cos k_n}{\sin k_n - \sinh k_n}, \tag{A.2}$$

and k_n the solutions of $\cos k_n \cosh k_n = 1$ sorted in ascending order such that $k_3 = 4.7300$, $k_4 = 7.8532$, etc.

Appendix A.2. Hydrodynamic lift and moment

The row vectors $\mathbf{l}$ and $\mathbf{m}$ needed to calculate the hydrodynamic lift and moment are given by

$$\mathbf{l}(k) = \left(C(k) + \frac{\mathrm{i}k}{2}, C(k), -\frac{\mathrm{i}k}{2}, 0\right), \tag{A.3}$$

$$\mathbf{m}(k) = \left(C(k), C(k) - 1 - \frac{\mathrm{i}k}{4}, -1, \frac{\mathrm{i}k}{4}\right), \tag{A.4}$$

where $C(k)$ is the Theodorsen function [14]

$$C(k) = \frac{H_1^{(2)}(k)}{H_1^{(2)}(k) + \mathrm{i}H_0^{(2)}(k)}, \tag{A.5}$$

with $H_n^{(2)}$ the Hankel function of the second kind.

Appendix A.3. Averaged thrust and energy

The $N \times N$ matrices needed to calculate the average energy loss, power required and leading-suction force are given by

$$\mathbf{E}(k) = B(k)\, \mathbf{F}^* \cdot \mathbf{F}, \tag{A.6}$$

$$\mathbf{P}(k) = -\frac{\mathrm{i}k}{2}\, \mathbf{G}^T \cdot \mathbf{F} + \frac{\mathrm{i}k}{2}\, \mathbf{F}^* \cdot \overline{\mathbf{G}}, \tag{A.7}$$

$$\mathbf{S}(k) = \mathbf{H}^* \cdot \mathbf{H}, \tag{A.8}$$

where the asterisk denotes the adjoint matrix and the bar the complex conjugate, with $B(k) = \Re(C(k)) - |C(k)|^2$,

$$\mathbf{F} = (\mathbf{r}_1 + \mathbf{r}_2) \cdot \mathbf{C}, \tag{A.9}$$

$$\mathbf{G} = (C(k)\mathbf{r}_1 + (1 - C(k))\mathbf{r}_2) \cdot \overline{\mathbf{B}}, \tag{A.10}$$

$$\mathbf{H} = (C(k)\mathbf{r}_1 - (1 - C(k))\mathbf{r}_2) \cdot \mathbf{C}, \tag{A.11}$$

and

$$\mathbf{r}_1 = (1, 0, 0, 0), \tag{A.12}$$

$$\mathbf{r}_2 = (0, 1, 0, 0). \tag{A.13}$$

References

[1] C. C. Lindsey, Form, function and locomotory habits in fish, in: W. S. Hoar, D. J. Randall (Eds.), Fish Physiology VII, Academic Press, 1978, pp. 1–100.

[2] M. Sfakiotakis, D. M. Lane, J. B. C. Davies, Review of fish swimming modes for aquatic locomotion, IEEE J. Oceanic Eng. 24 (1999) 237–252.

[3] G. V. Lauder, E. D. Tytell, Hydrodynamics of undulatory propulsion, Fish biomechanics 23 (2006) 425–462.

[4] T. Y.-T. Wu, Swimming of a waving plate, J. Fluid Mech. 10 (1961) 321–344.

[5] M. J. Lighthill, Aquatic animal propulsion of high hydromechanical efficiency, J. Fluid Mech. 44 (1970) 265–301.

[6] T. Y.-T. Wu, Hydromechanics of swimming propulsion. Part 1. Swimming of a two-dimensional flexible plate at variable forward speeds in an inviscid fluid, J. Fluid Mech. 46 (1971) 337–355.

[7] T. Y.-T. Wu, Hydromechanics of swimming propulsion. Part 2. Some optimum shape problems, J. Fluid Mech. 46 (1971) 521–544.

[8] T. Y.-T. Wu, Hydromechanics of swimming propulsion. Part 3. Swimming and optimum movements of slender fish with side fins, J. Fluid Mech. 46 (1971) 545–568.

[9] G. S. Triantafyllou, M. S. Triantafyllou, M. A. Grosenbaugh, Optimal thrust development in oscillating foils with application to fish propulsion, J. Fluids Struct. 7 (1993) 205–224.

[10] D. A. Read, F. S. Hover, M. S. Triantafyllou, Forces on oscillating foils for propulsion and maneuvering, Journal of Fluids and Structures 17 (2003) 163–183.

[11] L. Schouveiler, F. S. Hover, M. S. Triantafyllou, Performance of flapping foil propulsion, Journal of Fluids and Structures 20 (2005) 949–959.

[12] M. J. Lighthill, Note on the swimming of slender fish, J. Fluid Mech. 9 (1960) 305–317.

[13] M. J. Lighthill, Large-amplitude elongated-body theory of fish locomotion, Proc. R. Soc. Lond. B 179 (1971) 125–138.

[14] T. Theodorsen, General theory of aerodynamic instability and the mechanism of flutter, Technical Report TR-496, NACA, 1935.

[15] H. G. Küssner, I. Schwarz, The oscillating wing with aerodynamically balanced elevator, Technical Report TM-991, NACA, 1941.

[16] M. P. Paidoussis, Hydroelastic ichthyoid propulsion, J. Hydronaut. 10 (1976) 30–32.

[17] M. P. Paidoussis, Marine propulsion apparatus, US Patent 4129089, 1978.

[18] R. L. Bisplinghoff, H. Ashley, R. L. Halfman, Aeroelasticity, Dover, New York, 1983.

[19] C. Eloy, O. Doaré, L. Duchemin, L. Schouveiler, A unified introduction to fluid mechanics of flying and swimming at high Reynolds number, Exp. Mech. DOI 10.1007/s11340-009-9289-7 (2010).

[20] R. Godoy-Diana, J.-L. Aider, J. E. Wesfreid, Transitions in the wake of a flapping foil, Phys. Rev. E 77 (2008) 016308.

[21] C. Ellington, C. van den Berg, A. Willmott, A. Thomas, Leading-edge vortices in insect flight, Nature 384 (1996) 626–630.

[22] L. W. Carr, Progress in analysis and prediction of dynamic stall, J. Aircraft 25 (1988) 6–17.

[23] Wolfram Research, Inc., Mathematica edition: Version 7.0, 2008.

[24] M. G. Chopra, Large amplitude lunate-tail theory of fish locomotion, J. Fluid Mech. 74 (1976) 161–182.

[25] J. M. Anderson, K. Streitlien, D. S. Barrett, M. S. Triantafyllou, Oscillating foils of high propulsive efficiency, Journal of Fluid Mechanics 360 (1998) 41–72.

[26] F. E. Fish, J. J. Rohr, Review of dolphin hydrodynamics and swimming performance, Technical Report 1801, SSC San Diego, 1999.

[27] J. J. Rohr, F. E. Fish, Strouhal numbers and optimization of swimming by odontocete cetaceans, J. Exp. Biol. 207 (2004) 1633–1642.

[28] G. Taylor, R. L. Nudds, A. L. R. Thomas, Flying and swimming animals cruise at a Strouhal number tuned for high power efficiency, Nature 425 (2003) 707–711.

[29] M. G. Chopra, T. Kambe, Hydromechanics of lunate-tail swimming propulsion. part 2, J. Fluid Mech. 79 (1977) 49–69.

[30] J.-L. Guermond, A. Sellier, A unified unsteady lifting-line theory, J. Fluid Mech. 229 (1991) 427–451.

[31] C. Eloy, C. Souilliez, L. Schouveiler, Flutter of a rectangular plate, J. Fluids Struct. 23 (2007) 904–919.

[32] C. Eloy, R. Lagrange, C. Souilliez, L. Schouveiler, Aeroelastic instability of cantilevered flexible plates in uniform flow, J. Fluid Mech. 611 (2008) 97–106.